Antenna-Based Optical Imaging of Single Ca^{2+} Transmembrane Proteins in Liquids

Christiane Höppener and Lukas Novotny*

The Institute of Optics and Department of Biomedical Engineering, University of Rochester, Rochester, New York, 14627

ABSTRACT

Understanding the diversity of biological processes requires methods that can address single proteins in their natural environment and provide insights into structural and functional properties, as well as the local distribution of each individual protein. We use an optical antenna in the form of a single gold nanoparticle to localize incident laser radiation to 50 nm, significantly smaller than the diffraction limit of light. Our approach enables us to optically resolve individual plasma-membrane-bound Ca^{2+} pumps (PMCA4) immersed in aqueous environments and to determine the distribution of interprotein distances. We are able to correlate the protein maps with local topology. Improved antenna geometries will make it possible to resolve, identify, and probe single membrane proteins in live cells with true protein resolution of 5−10 nm.

Interprotein distances in cellular membranes fall generally in the regime below the diffraction limit of light due to their high density or their organization into specific regions, such as lipid rafts. Although atomic force microscopy (AFM) enables live cell imaging with atomic resolution,[1,2] it typically lacks the chemical specificity of optical imaging techniques based on fluorescence probes, for example, Förster resonance energy transfer (FRET), fluorescence correlation spectroscopy (FCS), fluorescence recovery after photobleaching (FRAP), and others.[3−5] Single-molecule fluorescence spectroscopy has opened the door for studying biological processes on a single protein level, but the resolution is typically limited by optical diffraction, making it impossible to address individual proteins in their native membrane. Recently, it has been shown that the diffraction barrier can be circumvented by making use of the photophysical properties of the target molecules.[6] For example, in the case of stimulated emission depletion (STED) microscopy,[7,8] resolution is enhanced by reversible saturable transitions. Such transitions are also used in saturated pattern excitation microscopy (SPEM).[9,10] The resolution in fluorescence microscopy can be increased even further by allowing only a subset of fluorescent molecules to be photoactive at a given time and ensuring that the nearest-neighbor distance between active molecules is larger than the diffraction limit. Methods that make use of this principle are photoactivatable localization microscopy (PALM)[11,12] and stochastic optical reconstruction microscopy (STORM).[13] In essence, these methods reconstruct an image molecule by molecule. The ascertainable localization accuracy depends strongly on the total number of photons being detected. However, so far, these techniques require long acquisition times.

Cells and biological membranes have also been imaged with near-field scanning optical microscopy (NSOM), which is able to resolve individual proteins.[14−19] NSOM makes it possible to measure optical properties (e.g., fluorescence) and the membrane topology simultaneously, thereby providing valuable information on the correlation between protein distribution and structural/mechanical properties of the membrane. Often, it is crucial to correlate the protein distribution with the membrane topology since the function and activity of specific membrane proteins can be influenced by their structural and chemical environment. Thus, details can be revealed on such topics as the role of lipid rafts in the formation and aggregation of specific membrane proteins, lipid bilayer dynamics, membrane protein assembly, membrane protein interactions, cellular dynamics, or mechanotransduction on cells, for example, in adhesion focals by simultaneous optical and topographical measurements.

Progress in the investigation of biological membranes and cells under physiological conditions by means of NSOM has been made due to the development of reliable and sensitive distance controls for noninvasive imaging in liquid environments.[20−22] However, so far, all of the reported biological applications in liquid environments are exclusively based on the use of circular aperture probes. The limitations of aperture probes (low transmission, low reproducibility, large physical size)[23] restrict the achievable optical resolution as well as

* To whom correspondence should be addressed. E-mail: novotny@optics.rochester.edu.
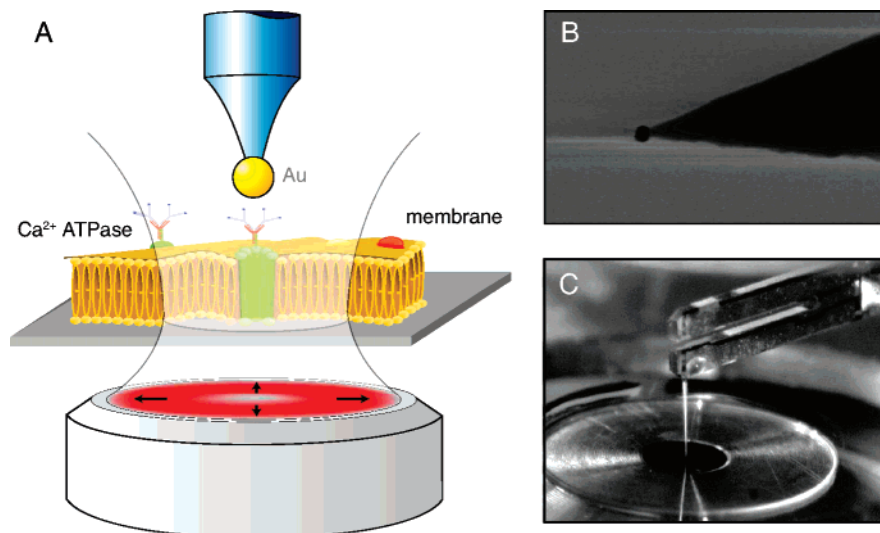
Figure 1. (A) Principle of antenna-based near-field optical microscopy. An optical antenna in the form of a single laser-irradiated gold nanoparticle[29,30] localizes incident laser radiation onto an erythrocyte plasma membrane with fluorescently labeled Ca^{2+} pumps (PMCA4). Fluorescence images of the membrane are recorded by raster scanning of the sample underneath the optical antenna while maintaining a constant separation between the antenna and sample, similar to standard scanning probe microscopy. (B) Electron micrograph showing an 80 nm gold particle attached to the tip of a pointed optical fiber. (C) Photograph showing the optical antenna mounted to a tuning fork and positioned into the focus of a microscope objective.

the ability to simultaneously measure the membrane topology. To overcome these barriers, so-called "tip-enhanced near-field optical microscopy" (TENOM) has been introduced.[24−28] In contrast to aperture-type NSOM, this technique is capable of achieving superior optical resolution, but the application to biological samples in physiological conditions has yet to be demonstrated. The laser-irradiated metal tip employed in TENOM can be viewed as a special type of optical antenna. It is important to emphasize that the optical antenna not only improves the resolution but also strongly reduces the photobleaching rate, as already demonstrated in the 70s by Hans Kuhn and co-workers.[32] Consequently, an optical antenna prolongs the lifetime of a fluorophore and opens the door to probe a single protein over an extended period of time. While the resolutions demonstrated in this article are on the order of 50 nm, it can be expected that improvements of the antenna geometry, material, and the illumination schemes will push this limit down to 10 nm in the future.[30]

As shown in Figure 1A, we use a laser-irradiated optical antenna composed of a single spherical gold nanoparticle to image individual proteins in a biological membrane. The base of the near-field optical setup is an inverted microscope with an integrated *xy*-scanning stage. A radially polarized laser beam with an excitation wavelength of $\lambda_{exc} = 633$ nm (He−Ne laser) exhibiting strong longitudinal fields is focused with an oil immersion objective of high numerical aperture (NA 1.4) on the surface. The optical antenna is positioned precisely in the laser focus and, thus, localizes the incident radiation and enhances the fluorescence rate of single molecules by a factor of 8−10.[29,30] An electron micrograph of a typical particle antenna is shown in Figure 1B, and Figure 1C depicts the antenna−sample region during operation. Fluorescence images are recorded by raster scanning of the optical antenna, in close proximity, over the sample

of interest and recording, pixel-by-pixel, the fluorescence rate with an avalanche photodiode. The tip−sample distance is controlled by means of a tapping-mode-like force feedback mechanism[31] based on a piezoelectric quartz tuning fork with a resonance frequency of ∼32.7 kHz (Figure 1C).

Here, we focus on the identification of single plasma-membrane-bound Ca^{2+} ATPases (PMCAs) in erythrocytes. These transmembrane proteins are part of the Ca^{2+} signalosome, which mediates parallel activation and inhibition of Ca^{2+}-dependent signaling pathways.[33] PMCAs regulate the cytosolic Ca^{2+} concentration in order to maintain Ca^{2+} homeostasis in cells. In erythrocytes, only the isoforms PMCA1 and PMCA4 are expressed, whereas PMCA4 is the predominant isoform. Approximately only every fourth PMCA pump is present in isoform 1.[34] Our antenna-based near-field optical approach allows us to resolve and identify single PMCA4 molecules to reveal their distribution in the membrane and to determine the interprotein distances, for the first time. Consequently, this technique opens up new possibilities to address issues like the identification of abnormalities in PMCAs regarding their integrity, activity, and interaction with effectors like calmodulin, caspases, or calpain, as well as the influence of structural and chemical changes in the membrane environment on a single protein level. An understanding of the underlying mechanisms of these transporters on a molecular scale is essential since abnormal remodeling of the Ca^{2+} signalosome has been observed in connection with several diseases, for example, hypertension, heart disease, diabetes, Alzheimer's disease, sickle cell anemia, muscular dystrophy, cystic fibrosis,[35,36] chronic kidney disease,[37]and even some cancers reveal characteristic alterations in the expression and activity of specific Ca^{2+} channels and pumps.[38] However, it remains still to be answered if dysfunction of Ca^{2+} transporters causes or just affects pathologic conditions in humans.

Erythrocyte plasma membranes were prepared similarly to the method described previously by Swihart et al.[39] Briefly, ~30 μl of human blood was diluted in 1 mL of 150 KH buffer (150 mM KCl, 20 mM HEPES, 24 mM sucrose, pH 6.9), and erythrocytes were isolated from human blood plasma by centrifugation. The isolated erythrocytes were deposited on 3-aminopropyltriethoxysilane (APTES, Alfa Aesar, U.S.A.) coated glass coverslips and incubated for 30 min in order to guarantee a tight adhesion to the substrate. Bright-field imaging of the samples performed after applying several washing steps showed that the surface was covered with a dense monolayer of cells. The remaining uncovered substrate areas were blocked using a KH buffer containing 2% bovine serum albumin (BSA). The erythrocytes were burst open by applying a low-concentration ionic buffer containing 5 mM NaH_2PO_4, 1 mM EDTA (pH 7.1), and 0.1% BSA at high pressure. In order to increase the accessibility of the antibodies to their cytoplasmic epitope binding region, the filamentous actin/spectrin mesh was removed by incubation with a 0.5 mM Na phosphate buffer (0.5 mM NaH_2PO_4, 0.05 mM EDTA, pH 7.4) at 37 °C for 2 h. For immunofluorescence staining, a mouse monoclonal antibody directed against the calcium pump PMCA4 was purchased from Abcam. This antibody (JA9) specifically recognizes PMCA4a and PMCA4b but is not specifically directed to the PMCA isoforms 1−3.[40] This primary antibody was diluted by 1:400 and applied over night at 4 °C, followed by thorough washing of the samples with the 5 mM Na phosphate buffer in an orbital incubator. The secondary goat anti-mouse antibody tagged with Alexa 633 dyes was added to the samples in a concentration of 1:1000 for 2 h at room temperature, followed by thorough washing of the samples in order to remove nonbound antibodies.

Erythrocyte membranes prepared following this procedure were imaged based on bright-field and confocal fluorescence imaging in order to adjust the preparation and immunofluorescence staining conditions. In addition, combined atomic force and confocal fluorescence microscopy performed simultaneously enabled us to correlate variations in the membrane topology with the fluorescence labeling efficiency. Bright-field and confocal fluorescence images of the samples reveal patterns with more or less uniform fluorescence efficiency but also patterns with suppressed fluorescence. The shape of the patterns is in accordance with the known diameter of intact erythrocytes of 6−8 μm.

Figure 2 displays a simultaneously acquired confocal fluorescence image and topographical AFM image of erythrocyte membranes deposited on a glass coverslip. The anticorrelation between the two images indicates that only single-layer membranes are fluorescent. The height of the fluorescent membranes is measured to be ~2 nm, as to be expected for a lipid bilayer after removal of the actin/spectrin mesh lining the cytoplasmic side of the erythrocyte plasma membrane. In contrast, the regions with suppressed fluorescence show an increased height of ~7 nm, indicating that these structures are not composed of a single lipid bilayer. In these cases, the epitope binding region of the PMCA protein on the cytoplasmic side of the membranes is not
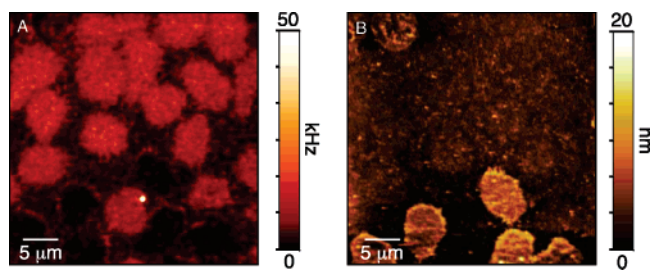

Figure 2. Imaging of erythrocyte membranes. (A) Confocal fluorescence image and (B) the simultaneously recorded topography of erythrocyte membranes deposited on a glass coverslip. Because PMCA transporter labeling is only efficient from the cytoplasmic side, only single-layer membranes exhibit fluorescence.

accessible to the antibody, resulting in a significantly lower staining efficiency. The residual fluorescence signal from these membranes corresponds to autofluorescence, as verified by measurements using unlabeled erythrocytes but prepared following the same procedure. Control experiments lacking an incubation with the primary antibody revealed negligible nonspecific labeling of the membranes. The reason for the occurrence of multiple-layer membranes is an imperfect bursting of the intact cell upon application of the lower-concentration ionic buffer, resulting in a collapse of the top membrane which then covers the cytoplasmic side of the bottom layer and hence prevents the access to the epitope binding site of the PMCA4 proteins. Our experiments are carried out exclusively on single-layer membranes with fluorescently labeled PMCA4 proteins.

The confocal fluorescence image in Figure 3A displays an area of densely arranged erythrocyte membranes. The resolution is on the order of 300 nm, and the fluorescence variations on single membranes indicate that the PMCA4 transporters do not allocate uniformly across the erythrocyte plasma membrane. Apparently, the interprotein distances of the PMCA4 enzyme are too small for single proteins to be resolved by means of confocal imaging, making it impossible to reveal the protein density and distribution (cf. Figure 3B). However, as shown in Figure 3C, imaging the same area with the gold nanoparticle antenna allows us to clearly resolve, for the first time, individual PMCA4 transporters in their native cell membranes. The optical resolution is determined by the size of the gold particle and is ~50 nm based on the full width at half-maximum (fwhm) of individual fluorescence spots (see inset). The fluorescence enhancement factor is ~8. Figure 3C shows that fluorescence spots from individual proteins are superimposed on a fluorescence background originating from the focused laser beam irradiating the optical antenna. Each PMCA4 protein in the confocal illumination area contributes to this confocal background, and thus, regions of higher protein abundance display a stronger background signal, which certainly can obscure image details for weak signals in these regions. Although not shown here, it is possible to separate the near-field fluorescence spots from the confocal background using simple Fourier filtering. Alternatively, the background can be eliminated during image acquisition using probe−sample distance modulation.[28]
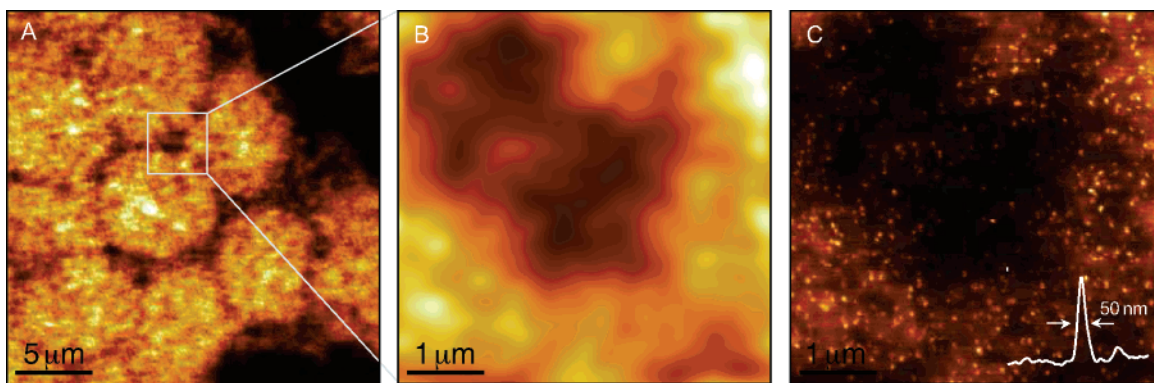
Figure 3. (A) Confocal fluorescence image of individual erythrocyte plasma membranes. (B) Close-up of the marked area in (A). The protein density is too high for individual proteins to be resolved confocally. (C) Near-field fluorescence image of the same area as that in (B) showing individually resolved PMCA4 transporters. The image was acquired with a ~60 nm gold nanoparticle antenna irradiated by a tightly focused radially polarized laser beam. The inset shows a cross section through one of the fluorescence spots, indicating a resolution of ~50 nm.

Measurements acquired in liquid show the same protein distribution and density as the measurements performed on dried membranes. The recorded near-field images are composed of isolated fluorescence spots, with a size limited by the resolution of the optical antenna. The secondary antibody used to label the proteins has multiple binding sites for the dye molecules. Consequently, each fluorescence spot is the result of several dye molecules. However, some fluorescence spots exhibit a characteristic orientation-dependent pattern, which originates from a single molecular transition dipole moment. We also find that the total number of fluorescence spots per erythrocyte coincides with previous estimates for the total number of PMCA4 transporters. Finally, we also recorded photobleaching time traces from single fluorescence spots and found an average of 2−4 photobleaching steps. Considering that the maximum number of dye molecules that can bind to the secondary antibody is six provides strong evidence that each fluorescence spot observed in our experiments is associated with a single PMCA4 protein.

Interestingly, we find that the distribution of proteins on single membranes is not uniform and that there is some minor background staining in the contact region between adjacent membranes (cf. Figure 3C), which might originate from nonspecific attachment of antibodies to the APTES-coated glass surface. However, the density is significantly lower than the protein density on the membranes. Figure 4A,B shows confocal and near-field fluorescence images of an erythrocyte membrane in liquid. In the near-field image, individual PMCA4 proteins are clearly resolved, although the signal-to-noise ratio is weaker compared with the dried membranes. Figure 4C shows a histogram of nearest-neighbor distances between PMCA4 proteins, revealing a rather broad distribution with an average of ~90 nm. We find membrane regions with a high PMCA4 density of ~30 proteins/μm that coexist with regions of lower density of ~20 proteins/μm.

PMCA4 is essential for Ca^{2+} homeostasis in erythrocytes. The ability to image the distribution of PMCA4 transporters in the plasma membrane is important for the understanding of expression levels, variations in activity, and abnormalities.

Recent studies indicate that certain PMCA4 isoforms are preferentially found in lipid rafts[41,42] and that their activity depends on the local environment, such as the presence of Ca^{2+}-specific effectors or oligomerization of the proteins. Measurements of PMCA4 distributions and their colocalization with other proteins in the plasma membrane are important for the development of therapeutic strategies against abnormalities in Ca^{2+} regulation and for a detailed understanding of signaling pathways and the mechanisms of activation and inhibition.

Here, we have shown that antenna-based near-field optical imaging makes it possible to resolve individual PMCA4 proteins in the plasma membrane, to measure the spatial protein distribution, and to reveal the difference in the protein density in various regions of the plasma membrane of erythrocytes. More generally, we have demonstrated for the first time that this technique is capable of high-resolution fluorescence imaging of biosamples in liquid environments.

The revealed PMCA4 distribution is composed of the specific isoforms PMCA4a and PMCA4b, which cannot be distinguished here since the applied primary antibody is specifically directed to a cytoplasmic epitope binding site, which is common to both isoforms. However, alternative staining protocols using isoform-specific antibodies allow one to also address PMCA4a and PMCA4b separately, and thus, it should be possible to image the distributions and to understand their colocalization. Colocalization studies of PMCA4a and PMCA4b or PMCA4 and PMCA1 are particularly interesting because varying PMCA properties might be associated with different isoforms[33] and thus reveal new insights into the Ca^{2+} transport mediated by PMCAs. The transport activity of these ion pumps can be further studied by colocalization studies of PMCA and specific Ca^{2+} effectors, for example, calmodulin.

In conclusion, antenna-based near-field microscopy opens up new perspectives for nanoscale bioimaging and single-molecule spectroscopy. Besides detailed colocalization studies, this technique makes it possible to correlate topological and optical information, which is important for a detailed understanding of the assembly and organization of biological membranes, specialized membrane regions such as lipid rafts,
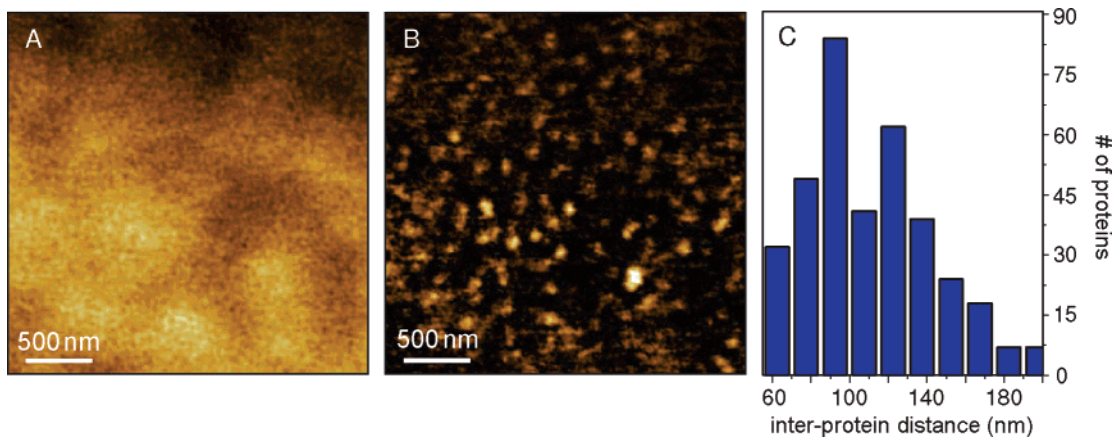
Figure 4. (A) Confocal fluorescence rate image of an erythrocyte plasma membrane immersed in H_2O. (B) Corresponding near-field fluorescence image showing individually resolved PMCA4 proteins. The image was acquired using an 80 nm gold nanoparticle antenna. The confocal background has been subtracted using high-pass filtering. (C) Distribution of nearest-neighbor interprotein distances, revealing an average protein−protein separation of 90 nm.

as well as membrane-associated structures, for example, the filamentous mesh lining the cytoplasmic side of the plasma membrane. The optimization of antenna geometries and materials will provide higher fluorescence enhancements and lead to true protein resolution (∼10 nm), allowing individual proteins of highest abundance to be imaged and monitored under physiological conditions.

References

(1) Radmacher, M.; Tillmann, R. W.; Fritz, M.; Gaub, H. E. *Science* **1992**, *257*, 1900−1905.
(2) Oesterhelt, F.; Oesterhelt, D.; Pfeiffer, M.; Engel, A.; Gaub, H. E.; Müller, D. J. *Science* **2000**, *288*, 143−146.
(3) Haustein, E.; Schwille, P. *Curr. Opin. Struct. Biol.* **2004**, *14*, 531−540.
(4) Weiss, S. *Science* **1999**, *283*, 1676−1683.
(5) Weiss, M.; Nilsson, T. *Trends Cell Biol.* **2004**, *14*, 267−273.
(6) Hell, S. W. *Science* **2007**, *316*, 1153−1158.
(7) Hell, S. W.; Wichmann, J. *Opt. Lett.* **1994**, *19*, 780−782.
(8) Donnert, G.; Keller, J.; Medda, R.; Andrei, A. M.; Rizzoli, S. R.; Lührmann, R.; Jahn, R.; Eggeling, C.; Hell, S. W. *Proc. Natl. Acad. Sci. U.S.A.* **2006**, *103*, 11440−11445.
(9) Heintzmann, R.; Jovin, T. M.; Cremer, C. *J. Opt. Soc. Am. A* **2002**, *19*, 1599−1609.
(10) Gustafsson, M. G. L. *Proc. Natl. Acad. Sci. U.S.A* **2005**, *102*, 13081−13086.
(11) Betizg, E.; Patterson, G. H.; Sougrat, R.; Lindwasser, O. W.; Olenych, S.; Bonifacino, J. S.; Davidson, M. W.; Lippincott-Schwartz, J.; Hess, H. F. *Science* **2006**, *313*, 1642−1645.
(12) Hess, S. T.; Girirajan, T. P. K.; Mason, M. D. *Biophys. J.* **2006**, *91*, 4258−4272.
(13) Rust, M. J.; Bates, M.; Zhuang, X. *Nat. Methods* **2006**, *3*, 793−795.
(14) Hwang, J.; Gheber, L. A.; Margolis, L.; Edidin, M. *Biophys. J.* **1998**, *74*, 2184−2190.
(15) Dunn, R. C.; Holton, G. R.; Mets, L.; Xie, X. S. *J. Phys. Chem.* **1994**, *98*, 3094−3098.
(16) Subramaniam, V.; Kirsch, A. K.; Jovin, T. M. *Cell. Mol. Biol.* **1998**, *44*, 689−700.
(17) Enderle, T.; Ha, T.; Chemla, D. S.; Weiss, S. *Ultramicroscopy* **1998**, *71*, 303−309.
(18) Dunn, R. C. *Chem. Rev.* **1999**, *99*, 2891−2928.
(19) Ianoul, A.; Street, M.; Grant, D.; Pezacki, J.; Taylor, R. S.; Johnston, L. J. *Biophys. J.* **2004**, *87*, 3525−3535.
(20) Höppener, C.; Siebrasse, J. P.; Peters, R.; Kubitscheck, U.; Naber, A. *Biophys. J.* **2005**, *88*, 3681−3688.
(21) Koopman, M.; Cambi, A.; de Bakker, B. I.; Joosten, B.; Figdor, C. G.; van Hulst, N. F.; Garcia-Parajo, M. F. *FEBS Lett.* **2004**, *573*, 6−10.
(22) Hwang, J.; Gheber, L. A.; Margolis, L.; Edidin, M. *Appl. Opt.* **1998**, *37*, 3574−3581.
(23) Hecht, B.; Sick, B.; Wild, U. P.; Deckert, V.; Zenobi, R.; Martin, O. J.; Pohl, D. W. *J. Chem. Phys.* **2000**, *112*, 7761−7774.
(24) Sánchez, E. J.; Novotny, L.; Xie, X. S. *Phys. Rev. Lett.* **1999**, *82*, 4014−4017.
(25) Frey, H. G.; Witt, S.; Felderer, K.; Guckenberger, R. *Phys. Rev. Lett.* **2004**, *93*, 200801−200804.
(26) Ichimura, T.; Hayazawa, N.; Hashimoto, M.; Inouye, Y.; Kawata, S. *Phys. Rev. Lett.* **2004**, *92*, 2208011−2208014.
(27) Neugebauer, U.; Rösch, R.; Schmitt, M.; Popp, J.; Julien, C.; Rasmussen, A.; Budich, C.; Deckert, V. *ChemPhysChem.* **2006**, *7*, 1428−1430.
(28) Ma, Z.; Gerton, J. M.; Wade, L. A.; Quake, S. R. *Phys. Rev. Lett.* **2006**, *97*, 260801−260804.
(29) Anger, P.; Bharadwaj, P.; Novotny, L. *Phys. Rev. Lett.* **2006**, *96*, 1130021−1130024.
(30) Rogobete, L.; Kaminski, F.; Agio, M.; Sandoghdar, V. *Opt. Lett.* **2007**, *32*, 1623−1625.
(31) Höppener, C.; Molenda, D.; Fuchs, H.; Naber, A. *J. Microsc.* **2003**, *210*, 288−293.
(32) Kuhn, H. *J. Chem. Phys.* **1970**, *53*, 101−108.
(33) Berridge, M. J.; Bootman, M. D.; Roderick, H. L. *Nat. Rev. Mol. Cell Biol.* **2004**, *4*, 517−529.
(34) Guerini, D.; Pan, B.; Carafoli, E. *J. Biol. Chem.* **2003**, *278*, 38141−38148.
(35) Carafoli, E. *Physiol. Rev.* **1991**, *71*, 129−153.
(36) Lew, V. L.; Bookchin, R. M. *Physiol. Rev.* **2005**, *85*, 179−200.
(37) Polak-Jonkisz, D.; Zwolińska, L.; Purzyc, L.; Musial, K. *Pediatr. Nephrol.* **2007**, *22*, 414−419.
(38) Monteith, G. R.; McAndrew, D.; Faddy, H. M.; Roberts-Thompson, S. J. *Nat. Rev. Cancer* **2007**, *7*, 519−530.
(39) Swihart, A. H.; Mikrut, J. M.; Ketterson, J. B.; McDonald, R. C. *J. Microsc.* **2001**, *204*, 212−225.
(40) Caride, A. J.; Filoteo, A. G.; Enyedi, A.; Verma, A. K.; Penniston, J. T. *Biochem. J.* **1996**, *316*, 353−359.
(41) Tang, D.; Deanb, W. L.; Borchmana, D.; Paterson, C. A. *Cell Calcium* **2006**, *39*, 209−216.
(42) Sepulveda, M. R.; Berrocal-Carrillo, M.; Gasset, M.; Mata, A. M. *J. Biol. Chem.* **2006**, *281*, 447−453.

NL073057T